



Article

A Method for Retrieving Cloud Microphysical Properties Using Combined Measurement of Millimeter-Wave Radar and Lidar

WeiQi Lin ¹ , Qianshan He ^{2,*}, Tiantao Cheng ^{1,3,4,5,6}, Haojun Chen ⁷, Chao Liu ⁷, Jie Liu ², Zhecheng Hong ², Xinrong Hu ² and Yiyuan Guo ²

¹ Department of Atmospheric and Ocean Science, Institute of Atmospheric Science, Fudan University, Shanghai 200433, China; 21213020010@m.fudan.edu.cn (W.L.)

² Shanghai Meteorological Service, Shanghai 200030, China; liu-jie@shmh.gov.cn (J.L.); huxinrong345091@cma.cn (X.H.)

³ Shanghai Key Laboratory of Ocean-Land-Atmosphere Boundary Dynamics and Climate Change, Fudan University, Shanghai 200433, China

⁴ Shanghai Frontiers Science Center of Atmosphere-Ocean Interaction, Fudan University, Shanghai 200433, China

⁵ CMA-FDU Joint Laboratory of Marine Meteorology, Fudan University, Shanghai 200438, China

⁶ Institute of Eco-Chongming (SIEC), Shanghai 202150, China

⁷ Shanghai Meteorological Information and Technology Support Center, Shanghai 200030, China

* Correspondence: oxeye75@gmail.com; Tel.: +86-189-1820-6010

Abstract: Clouds are an important component of weather systems and are difficult to effectively characterize using current climate models and estimation of radiative forcing. Due to the limitations in observational capabilities, it remains difficult to obtain high-spatiotemporal-resolution, continuous, and accurate observations of clouds. To overcome this issue, we propose a novel and practical combined retrieval method using millimeter-wave radar and lidar, which enables the microphysical properties of thin liquid water clouds, such as cloud droplet effective radius, number concentration, and liquid water content, to be retrieved. This method was utilized to analyze the clouds observed at the Shanghai World Expo Park and was validated through synchronous observations with a microwave radiometer. Furthermore, the most suitable extinction backscatter ratio was determined through sensitivity analysis. This study provides vertical distributions of cloud microphysical properties with a time resolution of 1 min and a spatial resolution of 30 m, demonstrating the scientific potential of this combined retrieval method.

Keywords: cloud; combined retrieval; microphysical properties



Citation: Lin, W.; He, Q.; Cheng, T.; Chen, H.; Liu, C.; Liu, J.; Hong, Z.; Hu, X.; Guo, Y. A Method for Retrieving Cloud Microphysical Properties Using Combined Measurement of Millimeter-Wave Radar and Lidar. *Remote Sens.* **2024**, *16*, 586. <https://doi.org/10.3390/rs16030586>

Academic Editor: Matthew McGill

Received: 17 December 2023

Revised: 22 January 2024

Accepted: 30 January 2024

Published: 4 February 2024



Copyright: © 2024 by the authors. Licensee MDPI, Basel, Switzerland. This article is an open access article distributed under the terms and conditions of the Creative Commons Attribution (CC BY) license (<https://creativecommons.org/licenses/by/4.0/>).

1. Introduction

More than 60% of the Earth's surface is covered by clouds [1], which play a crucial role in simulating the Earth's climate system and predicting climate change [2–4]. Additionally, clouds regulate the energy balance of the Earth–atmosphere system by influencing surface longwave radiation and solar shortwave radiation [5,6]. The Intergovernmental Panel on Climate Change (IPCC) has identified clouds as one of the largest sources of uncertainty in climate predictions and estimates of total radiative forcing [7]. To better quantify the role of clouds in these processes, a clearer understanding of the microphysical properties of clouds is needed.

Millimeter-wave radar (MMWR) is a radar system that uses the millimeter-wave frequency range for detection and measurement. The detection of clouds by satellites is usually achieved through threshold-based segmentation. However, the complex composition of the land surface and the high variability of reflectivity in different cloud types can lead to biased detection results [8], and cloud masks are an important basis for estimating cloud amount [9]. In addition, satellites can typically only retrieve the macro- and micro-characteristics of cloud tops and have much longer revisit times compared to the

time scale of cloud changes [10,11]. Unlike satellites, MMWR is capable of effectively penetrating cloud layers with minimal interference from atmospheric turbulence and ground echoes. It can continuously observe the macro-parameters of clouds while also capturing information about the structure and motion of particles within the clouds [12,13]. Aircraft and radiosonde balloons can collect the microphysical properties of cloud particles, but they are limited by weather conditions and cost [14]. In contrast, MMWR can provide uninterrupted real-time monitoring of vertical profile changes in clouds, thereby compensating for the limitations of the remote sensing methods mentioned above. Lidar, on the other hand, is a powerful tool in the study of the optical properties of clouds using laser beams. It can directly measure aerosol characteristics below the cloud base and liquid droplet microphysical properties above the cloud base [15]. Therefore, it is necessary to combine the advantages of existing meteorological instruments to achieve all-weather, automated, and high-precision cloud observations.

Lidar with smaller wavelengths can effectively detect aerosols ranging from a few nanometers to a few micrometers in size but may overlook cloud droplets in the tens-of-micrometers range [16]. Radar reflectivity strongly depends on the sixth power of cloud droplet diameter and is not sensitive to small cloud droplets [17]. This can lead to MMWR with longer wavelengths being unable to detect small particles in cloud droplet clusters, resulting in the loss of small liquid droplets in the cloud droplet spectrum. The combination of MMWR and lidar can more fully detect all particles in a cloud droplet cluster and more accurately identify cloud boundaries. This is why MMWR and lidar are combined for retrieve purposes. On this basis, the ratio of MMWR-to-lidar backscatter power is a sensitive function of mean size. Once the size is known, the other microphysical properties of a cloud can be further derived. However, this technology may only be applicable to a few hundred meters above the base of thin clouds or thick clouds, as once the lidar penetrates the cloud layer, it will be attenuated, resulting in a small received signal and affecting the retrieval results.

Numerous studies have demonstrated the effectiveness of combining radar and lidar to retrieve cloud microphysical properties. The physical basis for such an approach was first explored by Intrieri et al., who combined an 8.6 mm Doppler radar, 3.2 cm Doppler radar, and CO₂ lidar to retrieve the particle sizes of cirrus clouds [18]. On this basis, Mitrescu et al. established a lidar–radar model to account for the nonspherical effects of ice crystals and laser attenuation and improved the traditional optimal estimation retrieval method to retrieve the microphysical properties of cirrus clouds [19]. Protat et al. compared the microphysical characteristics of ice clouds retrieved from ground-based radar and lidar with satellite data to evaluate the ice microphysical products of CloudSat and CALIPSO [20]. Vivekanandan used measurement data from radar and lidar to retrieve the droplet diameter and liquid water content of stratocumulus clouds through electromagnetic simulation [21]. Similar papers followed, such as those of Heymsfield et al. and Delanoë et al. [22,23].

The above radar–lidar methods suffer from the following limitations: (1) Most of them rely on prior assumptions about the cloud droplet spectrum, such as gamma distribution. (2) They only used the backscatter coefficient of lidar but not the extinction coefficient. In this paper, we combine Ka-band MMWR and 532 nm lidar to retrieve the microphysical properties of clouds. The two main objectives of this study are (1) to estimate the effective radius (R_e) of cloud droplets through the backscatter coefficients measured by the MMWR and lidar, without assuming the spectral distribution of cloud droplets, and (2) to calculate cloud droplet number concentration (N_d) and liquid water content (LWC) using the R_e and extinction coefficients retrieved by the lidar.

2. Materials and Methods

2.1. Instruments

The instruments used in this study included a 35 GHz Ka-band ground-based MMWR, a micro-pulse lidar, and a microwave radiometer from the Shanghai World Expo Park. The straight-line distance between the three was within 20 m. The Shanghai World Expo

Park is located at 31.19°N and 121.50°E, along both banks of the Huangpu River, and the surrounding buildings are mainly commercial and residential areas.

The three instruments underwent a seven-month observation period from June to December 2020 and from May to November 2021. During the 2020 period, the MMWR and microwave radiometer operated normally, but the lidar was unable to obtain valid data from June to October 2020 due to insufficient laser emission power. After updating the laser, valid data were obtained. In 2021, both the MMWR and lidar operated normally, but the microwave radiometer experienced a malfunction from 16 September to 30 November 2021. During this period, no data could be obtained for some time, or even for the entire day, for level 2 files each day.

The MMWR used in this study was the HMB-KPS model manufactured by Beijing Institute of Radio Measurement, with a working wavelength of 8.57 mm and a zenith observation mode with an elevation angle of 90° (Figure 1). It has a maximum detection range of 20 km. This radar has high sensitivity, with a precision of 0.01 dBZ in its reflectivity factor and 0.01 m/s for radial velocity and spectral width. It also has high spatiotemporal resolution, acquiring a data file every minute with a range resolution of 30 m. Gossard and Tao used power spectral data from MMWR to retrieve cloud droplet spectra and cloud microphysical properties through deconvolution and optimal cost function spectral separation technology, respectively [24,25].



Figure 1. Photo of HMB-KPS millimeter-wave radar.

The lidar used in this study was the MPL-4B-IDS series micro-pulse lidar produced by Sigma Space Corporation, with a wavelength of 532 nm and consistent spatiotemporal resolution, distance resolution, observation mode, and maximum observation range with the MMWR (Figure 2). It can be used to retrieve atmospheric extinction coefficient profiles, aerosol optical thickness, cloud base height, and planetary boundary layer height. Under the constraint of measured aerosol optical depths, He et al. used micro-pulse lidar to retrieve the column-averaged aerosol extinction-backscatter ratio in Hong Kong [26].



Figure 2. Photo of MPL-4B-IDS micro pulse lidar.

The microwave radiometer used in this study was produced by Radiometrics Corporation in Boulder, CO, USA and was composed of three parts: TP/WVP-3000, TP-2500, and WVP-1500 (Figure 3). It can retrieve atmospheric temperature, water vapor density, LWC, and relative humidity in the height range of 0–10 km, encompassing 57 layers. Subsequently, the liquid water path (LWP) can be calculated. The microwave radiometer has a time resolution of 1–2 min and a vertical resolution between 50 and 250 m. Due to the disparate spatiotemporal resolutions of the two radars and the microwave radiometer, pre-processing of the data from all three instruments is required before retrieving the cloud microphysical properties. A method comparing LWP rather than LWC was used to eliminate the influence of distance resolution. Radar data that closely matched the microwave radiometer data were selected for temporal alignment.



Figure 3. Photo of microwave radiometers produced by Radiometrics Corporation.

2.2. Retrieval of MMWR

In general, the retrieval of cloud microphysical properties by MMWR is based on power spectral data or base data. Power spectral data refers to the function of the power of particle backscatter in the radar sample library versus their velocity, while base data are spectral moment parameters such as radar reflectivity factor, velocity, and spectral width obtained after the signal processing of the original signal. Using the method proposed by Huang et al. [27], assuming the cloud droplet spectrum distribution as a gamma distribution under Rayleigh scattering conditions, the cloud droplet spectrum distribution can be represented as:

$$n(D) = N_0 D^\mu e^{-\lambda D} \quad (1)$$

where N_0 is the gamma distribution parameter, D is the diameter of the cloud droplet, μ is the shape parameter in the gamma distribution, and λ is the slope in the gamma distribution. Subsequently, Re , N_d , and LWC are expressed using the moment method as follows:

$$Re = \frac{\int n(r)r^3 dr}{\int n(r)r^2 dr} = \frac{3 + \mu}{\lambda} \quad (2)$$

$$N_d = \int n(D)dD = \frac{\mu! \times N_0}{\lambda^{1+\mu}} = \frac{\mu! \times \lambda^6}{(6 + \mu)!} \times Z \quad (3)$$

$$LWC = \frac{4\pi\rho_w}{3} \int n(r)r^3 dr = \frac{\pi\rho_w}{6} \times \frac{(3 + \mu)!}{(6 + \mu)!} \times Z\lambda^3 \quad (4)$$

where Z is the radar reflectivity factor and ρ_w is the density of liquid water. There are two unknowns left in the above equation: μ is generally assumed to be 0 in stratus, and λ can be expressed using Melchionna's calculation of the cloud particle vertical velocity [28]:

$$\lambda = \left(\frac{a^2}{\sigma_d^2} \times \left(\frac{\Gamma(2b + \mu + 7)}{\Gamma(7 + \mu)} - \left(\frac{\Gamma(b + \mu + 7)}{\Gamma(7 + \mu)} \right)^2 \right) \right)^{\frac{1}{26}} \quad (5)$$

where a and b are dimensionless empirical parameters in the empirical relationship between cloud particle diameter and fall velocity, with values of 2.975×10^5 and 2 , respectively. σ_d represents the spectral width, and Γ denotes the gamma function. In this way, the cloud microphysical characteristics can be retrieved from the base data of the MMWR.

2.3. Combined Retrieval

Scattering refers to the process in which electromagnetic waves pass through a certain medium and, due to the non-uniform refractive index of the medium, cause disturbances in the wavefront of the incident wave. This results in a portion of the energy of the incident wave deviating from the original propagation direction and being emitted in a certain pattern towards other directions. The scattering process can be classified based on the following scale parameters:

$$\alpha = \frac{2\pi r}{\lambda} \quad (6)$$

where r is the particle radius and λ is the wavelength. When $\alpha \ll 1$, scattering is described as Rayleigh scattering. When $\alpha \approx 1$ or $\alpha > 1$, scattering is described as Mie scattering. The difference in backscattered returns from instruments widely separated in a wavelength can provide information on the characteristic sizes of the scatterers. Using the method proposed by Intrieri et al., the Re of cloud particles can be remotely determined by combining the backscatter data from both the MMWR and lidar [18]. Stephens assumed a gamma distribution for the cloud droplet spectrum when calculating the theoretical backscatter coefficients of the MMWR and lidar. However, we directly calculated the backscatter coefficients based on the scattering function, employing a method introduced by Welton to compute the observed backscatter coefficients of the lidar instead of the differential backscatter cross section. This section uses Rayleigh scattering theory to calculate the radar backscatter coefficient, while using Mie scattering theory to calculate the lidar backscatter coefficient.

2.3.1. Calculation of Theoretical Backscattering Coefficient

For Rayleigh scattering, the scattering function is:

$$\sigma(\theta) = \frac{8\pi^4 r^6}{\lambda^4} \left(\frac{m^2 - 1}{m^2 + 2} \right)^2 (1 + \cos^2\theta) \quad (7)$$

where $m = n - in'$ represents the complex refractive index of the medium in which n is the real part, defined as the refractive index, and n' is defined as the internal absorption within the particles. In general, the refractive index of atmospheric aerosols ranges from 1.33 to 1.60 [29]. θ is the angle between the incident light and the observation direction, which is also known as the scattering angle. When the scattering angle is 180 degrees, the equation above represents the backscattering coefficient:

$$\sigma_{\text{radar}} = \frac{16\pi^4 r^6}{\lambda^4} \left(\frac{m^2 - 1}{m^2 + 2} \right)^2 \quad (8)$$

For Mie scattering, the formula for the scattering phase function is:

$$P(\theta) = \frac{|S_1(\theta)|^2 + |S_2(\theta)|^2}{\sum_{n=1}^{\infty} (2n + 1) (|a_n|^2 + |b_n|^2)} \quad (9)$$

where $S_1(\theta)$ and $S_2(\theta)$ are complex amplitude functions. a_n and b_n are complex functions known as Mie scattering parameters, which reflect the influence of electric field oscillations and magnetic field oscillations on scattering. They are determined by the complex refractive index m , the size parameter α , and the parameter $m\alpha$ of the particles. When θ is 180 degrees, the theoretical backscattering coefficient of the lidar can be calculated as:

$$\sigma_{\text{lidar}} = P(180^\circ) \quad (10)$$

2.3.2. Calculation of Observed Backscattering Coefficient

The relationship between the radar reflectivity factor Z and effective reflectivity factor Z_e is:

$$Z_e = 10^{0.1Z} \quad (11)$$

Then, we can calculate the observed backscattering coefficient of the MMWR as follows:

$$\beta_{\text{radar}} = Z_e \left(\frac{m^2 - 1}{m^2 + 2} \right)^2 \frac{\pi^5}{\lambda^4} \quad (12)$$

To determine the aerosol backscatter coefficient β_a and extinction coefficient α_c . Welton's method was employed using the independently observed aerosol optical thickness τ as a constraining factor for the retrieval of the lidar signal [30]:

$$\beta_a(x-1) = \frac{X(x-1)\Psi(x-1, x)}{\frac{X(x)}{\beta_a(x) + \beta_m(x)} + 2S_a\{X(x) + X(x-1)\Psi(x-1, x)\}\Delta z} - \beta_m(x-1) \quad (13)$$

where x is the range and x is one distance resolution higher than $x-1$, $X(x) = P(x) \cdot x^2$, where $P(x)$ is the return signal, $\Psi(x-1, x) = \exp[(S_a - S_m)(\beta_m(x-1) + \beta_m(x))\Delta z]$, where S_a is the aerosol extinction backscatter ratio, $S_m = (8\pi/3)$ is the molecular extinction backscatter ratio, and Δz is the distance resolution of the lidar. Assuming S_a has an initial value, by using an iterative algorithm to approach $S_{\text{anew}} (<0.5\%)$, we can obtain the final backscatter coefficient β_{lidar} at various heights. The software developed by He was used to process the lidar data in this paper [31].

In this study, the theoretical and observed backscatter coefficients need to be compared, so it was necessary to define the following ratios:

$$\gamma_t = \frac{\sigma_{\text{radar}}}{\sigma_{\text{lidar}}} \quad (14)$$

for theory and

$$\gamma_o = \frac{\beta_{\text{radar}}}{\beta_{\text{lidar}}} \quad (15)$$

for observation. It is notable that γ_t and γ_o can be directly compared.

Figure 4 shows the theoretical backscattering coefficient ratio of the Ka-band radar and 532 nm lidar for a refractive index of $1.43 + 0.0005 \times i$. Given that cloud droplet sizes are typically within the range of a few micrometers to several tens of micrometers, we restricted the range of Re from 0 to 100 micrometers. The values of the ratio γ_t range from 10^{-14} to 10^{-4} from the small to the large end of the range in Re . Distributions characterized by small values of Re are associated with low ratios, while those with large values of Re are associated with higher ratios. Compare the ratio γ_o obtained from simultaneous measurements of radar and lidar in the field with the curve in Figure 4 to yield the experimental Re .

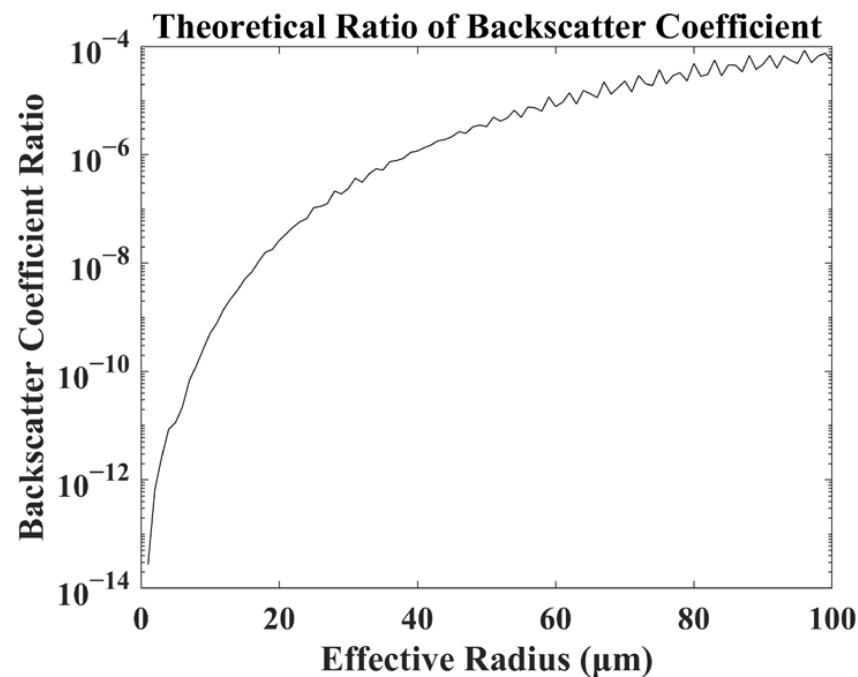


Figure 4. Log of the radar–lidar backscatter coefficient ratios versus Re for the Ka-band radar over 532 nm lidar.

2.3.3. Calculation of LWC and N_d

Previous studies have concluded that the basic characteristics of liquid water cloud layers include not only the Re but also the N_d , as well as the extinction coefficient of cloud droplets (single scattering) α_c and the LWC [32,33]. The calculation formulas for N_d , LWC, and LWP are also provided as follows:

$$LWC = \frac{2}{3} \rho_w \alpha_c Re \quad (16)$$

$$N_d = \frac{\alpha_c}{2\pi k Re^2} \quad (17)$$

$$LWP = \int_0^{\infty} LWC(z) dz = \sum_{i=1}^n [\Delta z \times LWC(z_i)] \quad (18)$$

where k is the ratio of the cube of the effective radius of cloud droplets to the cube of the volume average droplet radius; Lu summarized the previous studies and found that when the value of k is within the range of 0.75 ± 0.15 [34], it can better represent continental cloud clusters.

It is worth noting that in previous studies, the extinction coefficient obtained from the narrow-field channel of a dual-field-of-view lidar was used as the initial value for α_c and iteratively obtained the final α_c value. In this study, however, the extinction coefficient was obtained using Welton's method. Additionally, we used the method described earlier to obtain the effective radius of cloud droplets instead of converging it to the minimum cost function by providing an initial value.

3. Results

The evaluation and verification of retrieval quality are mainly conducted by assessing the retrieval of cloud microphysical properties and comparing them with other relatively reliable detection results. Microwave radiometers are considered to be a more accurate method for detecting the LWP in clouds, with a 1 K brightness temperature deviation resulting in an approximate 30 g/m^2 deviation in the retrieval of the LWP by the microwave

radiometer [35]. Since there were no aircraft measurement data available to compare the Re and Nd of cloud droplets and satellite products can only provide cloud top data rather than vertical profiles, we viewed the LWP retrieved from ground-based microwave radiometers as the truth [36]. Subsequently, the influence of different extinction backscatter ratios on LWP in combined retrieval was analyzed.

3.1. Stratus

Figure 5a shows the radar reflectivity factor observed by the MMWR on 1 November 2020. Complex multi-cloud conditions were observed, including dual-layer clouds from 5:00 to 5:50, single-layer clouds from 5:50 to 6:15, and dual-layer clouds from 6:15 to 7:00. The overall echo intensity of this cloud event was relatively weak, mostly below -10 dBZ. The cloud top height of the upper layer was 5.5 km with a cloud thickness of 1 km, while the cloud top height of the lower layer was 3.3 km with a cloud thickness of several hundred meters.

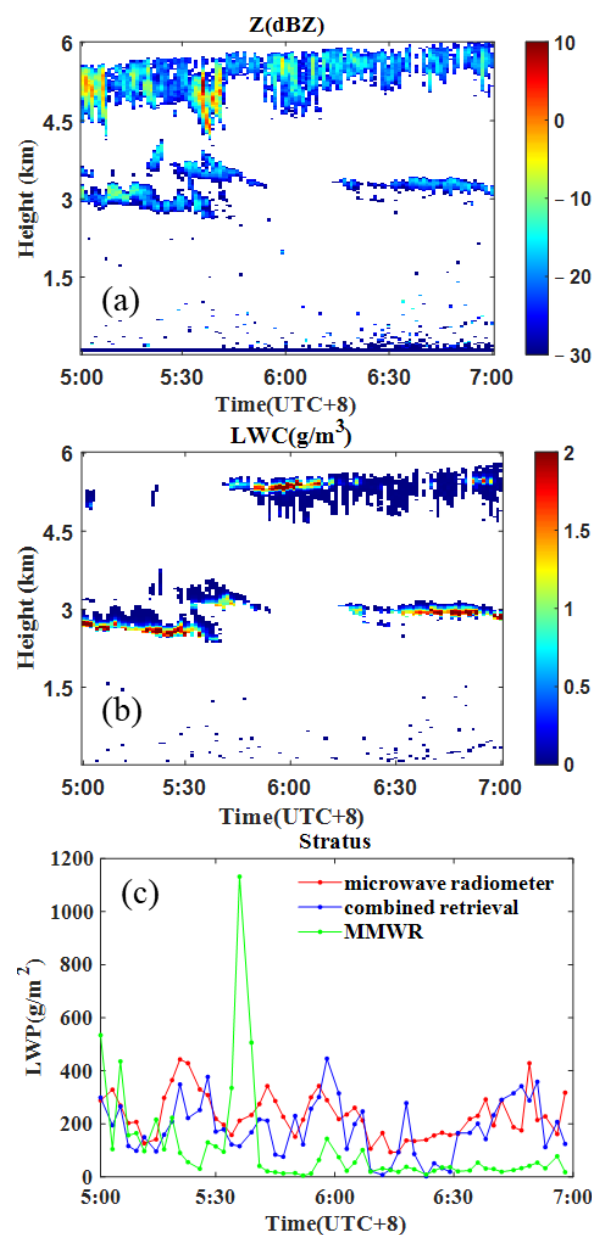


Figure 5. Verification of retrieval results of stratus clouds observed at the Shanghai World Expo Park on 1 November 2020 for (a) radar reflectivity factor, (b) LWC obtained through combined retrieval, and (c) comparison of LWP between microwave radiometer, MMWR, and combined retrieval.

Figure 5c compares the LWPs retrieved by the MMWR, combined retrieval, and microwave radiometer methods during the stratus cloud process. The LWP retrieved by the MMWR showed a large deviation from the truth, with a correlation coefficient r of only 0.04 and a mean absolute percentage difference (MAPD) of 82.82%. Conversely, the LWP derived from the combined retrieval exhibited a good overall consistency with the truth in terms of trends, with an r reaching 0.51 and a MAPD of 41.26%. When retrieving the LWP using MMWR, it relies on the spectral width and radar reflectivity factor. However, air disturbances can have a certain impact on the spectral width, leading to large fluctuations in the inversion results. Additionally, differences in the radar reflectivity factor for certain dBZ values can result in significant variations in the inversion results. To address these issues, the combined retrieval of LWP takes into account the effective radius and extinction coefficient. Obtaining reliable values for these parameters can make the retrieval results closer to the true values. Figure 5b shows the LWC results from the combined retrieval method, which demonstrate that the lidar cannot penetrate thick cloud layers, resulting in no LWC retrieval results in that region. This could be one of the reasons why the retrieved LWP was underestimated compared to the true values. It is worth noting that, considering the positional discrepancies between the MMWR, lidar, and microwave radiometer, after adjusting the results of the combined retrieval by one time step (about one minute) forward, the r improved to reach 0.57, and the MAPD decreased to 37.35%.

Sensitivity analysis based on the extinction backscatter ratio was designed for the LWP obtained from the combined retrieval method, and the extinction backscatter ratio was increased from 30 to 70 in increments of 10 (Figure 6). As the extinction backscatter ratio increased, the LWP obtained from combined retrieval gradually increased, and the two were positively correlated. Table 1 provides a sensitivity analysis of the extinction backscatter ratio based on this stratus process, compared with the LWP data obtained from the microwave radiometer. For different extinction backscatter ratios, the r values of the LWP obtained by the combined retrieval and microwave radiometer methods were the same, but there were slight differences in MAPD and root mean square error (RMSE). Overall, when the extinction backscatter ratio was 40, the LWP obtained by combined retrieval under stratus clouds had the best consistency with the true value.

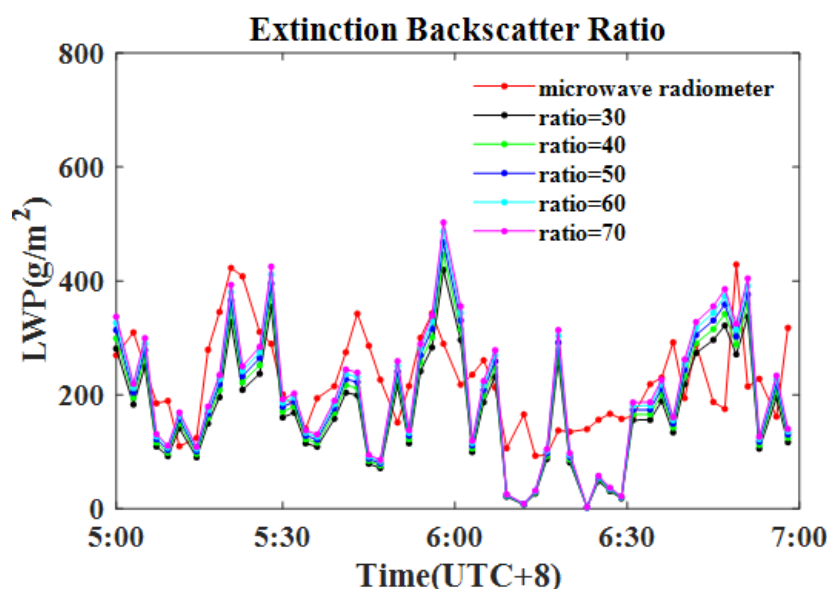


Figure 6. Sensitivity analysis based on the LWP of the stratus process on 1 November 2020 for extinction backscatter ratio.

Table 1. Summary of the comparison between the LWPs calculated using different backscatter ratios in combined retrieval and the true values.

Variable	Backscatter Ratio	Stratus			Cumulus		
		r	MAPD	RMSE	r	MAPD	RMSE
Backscatter ratio	30	0.51	41.56%	104.51	0.52	79.44%	605.77
	40	0.51	41.26%	102.96	0.52	78.51%	597.33
	50	0.51	41.59%	102.82	0.52	77.80%	590.53
	60	0.51	41.92%	103.52	0.52	77.27%	584.82
	70	0.51	42.20%	104.75	0.52	76.88%	579.87

3.2. Cumulus

The same method was used to analyze the accuracy and sensitivity of combined retrieval results under cumulus conditions. On 6 October 2021, the MMWR and lidar observed discontinuous cumulus weather at the Shanghai World Expo Park between 19:30 and 22:00. Figure 7a shows the radar reflectivity factor observed by the MMWR. The overall echo intensity of this cloud process was relatively high, mostly above -10 dBZ, and reached a maximum of 12.46 dBZ. The cloud top height was about 4 km, with a maximum thickness of 2 km.

Figure 7c shows the comparison of the LWPs retrieved by the MMWR, combined retrieval, and microwave radiometer methods during the stratus cloud process. There is a significant discrepancy between the LWP retrieved by the MMWR and the truth. The r is -0.19 and does not even show a positive correlation, with a MAPD reaching 149.79%. On the contrary, the LWP derived from the combined retrieval exhibits a good overall consistency with the truth in terms of trends, with an r reaching 0.52 and a MAPD of 78.51%. Similarly, after adjusting the results in terms of time, the r improves to 0.54 while the MAPD remains relatively unchanged. The results of the combined retrieval are lower than the true value, which is attributed to the thick cumulus layer limiting the penetration of lidar signals, resulting in the absence of LWC retrieval results in some areas (Figure 7b) and leading to lower LWP retrieval results and deviation from the truth.

Overall, when observing thin layer clouds, the LWP obtained from combined retrieval showed reasonable consistency in trends and numerical values with the measurement results of microwave radiometers. When observing thick cumulus clouds, the LWP obtained from combined retrieval had a relatively consistent trend with the measurements of the microwave radiometer, but the numerical value was far underestimated. Therefore, this technology may only be applicable to a few hundred meters above the base of thin clouds or thick clouds, and the cloud microphysical properties obtained through combined retrieval within this range are generally reliable. For clouds with a thickness of several thousand meters or even tens of kilometers, further research on their microphysical characteristics is needed in the future.

The influence of the extinction backscatter ratio on the LWP obtained with the combined retrieval method under cumulus clouds is consistent with that of stratus clouds (Figure 8). As the extinction backscatter ratio increases, the LWP also increases accordingly. Table 1 reveals that when the extinction backscatter ratio was 70, the combined retrieval effect was the best for cumulus clouds. However, as discussed earlier, the LWP obtained from combined retrieval should be smaller than the true value, and there is a significant deviation between the two. Undoubtedly, blindly increasing the extinction backscatter ratio can make the combined retrieval results closer to the true value, but it does not match the actual situation. Therefore, when conducting combined retrieval of cumulus clouds, the same extinction backscatter ratio as in the case of stratus clouds was selected, which is 40.

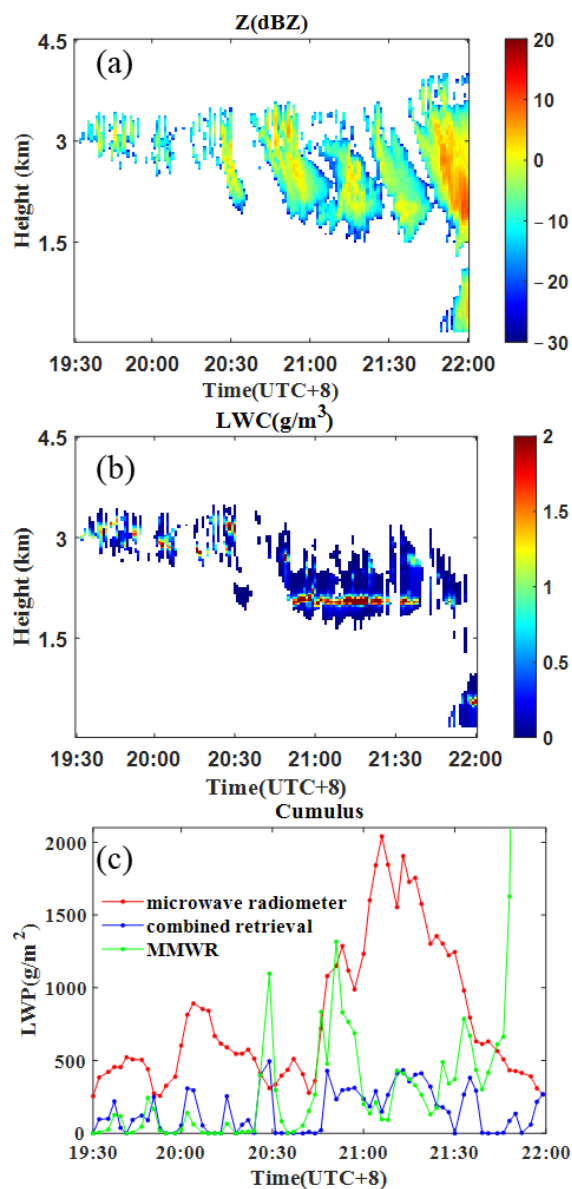


Figure 7. Verification of retrieval results of cumulus clouds observed at the Shanghai World Expo Park on 6 October 2021 for (a) radar reflectivity factor, (b) LWC obtained through combined retrieval, and (c) comparison of LWP between microwave radiometer, MMWR, and combined retrieval.

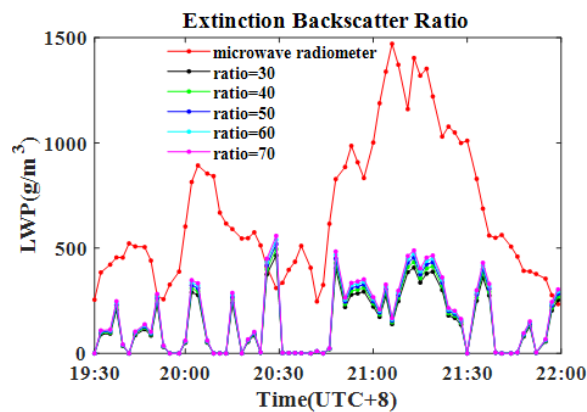


Figure 8. Sensitivity analysis based on LWP for the cumulus process on 6 October 2021 for extinction backscatter ratio.

4. Discussion

We now apply the technique described in Section 2 to data obtained by the HMB-KPS MMWR and MPL-4B-IDS micro-pulse lidar at the Shanghai World Expo Park. Given that the lidar cannot penetrate thick cloud layers, resulting in an underestimation of retrieval values for cumulus, this study selects stratus with relatively thin cloud layers and uniformly distributed droplet sizes for investigation. The retrieval results were validated in Section 3.1 through a stratus process on 1 November 2020. Now, we further analyze their microphysical properties.

The derived microphysical properties are displayed in Figure 9. Figure 9b shows the vertical distribution of cloud droplets Re obtained by combined retrieval with a resolution of 1 min and 30 m, with most cloud droplets having an Re of less than $5 \mu\text{m}$, and the maximum value was $28.74 \mu\text{m}$. The high values of Re at the top of the lower layer clouds were mainly due to collision and coalescence caused by updrafts as shown in Figure 9a. It is worth noting that relatively lower values of Re often occur simultaneously with higher values of N_d and LWC , which is similar to the results obtained by Wang et al. using dual-field-of-view high-spectral-resolution lidar to retrieve the microphysical properties of water clouds in Beijing [37].

The vertical distribution of cloud droplets N_d is shown in Figure 9c; high-value areas of N_d usually appear together with low-value areas of Re and may be attributed to the negative correlation between N_d and Re (Equation (17)). In addition, the accuracy of the combined retrieval results of N_d remains to be debated. Previous studies have shown that the uncertainty of N_d calculated by this method ranges from 25% to 75% [38].

Figure 9d shows the vertical distribution of cloud droplet LWC , with the median LWC being 0.03 g/m^3 and the average value of 0.33 g/m^3 demonstrating that the LWC of most cloud droplets is relatively small, but there are several larger values. Previously, it was calculated that the LWP of this cloud process ranges from 100 to 400 g/m^2 , which is a characteristic of typical stratocumulus [39]. Overall, the aforementioned microphysical characteristics of clouds are typical of non-precipitating low-level water clouds in polluted continental or marine environments [40].

Table 2 provides the retrieved microphysical properties of different cloud types observed at the Shanghai World Expo Park from May to November 2021 (particles with Re less than $2.5 \mu\text{m}$ were considered aerosol particles and excluded). The average Re of cloud droplets was $7.91 \mu\text{m}$, the average N_d was 3059 cm^{-3} , and the average LWC was 0.28 g/m^3 . Warm and moist air is lifted slowly by cold air and undergoes adiabatic cooling and condensation, forming nimbostratus. The vigorous convective motions inside the clouds accelerate the growth of cloud droplets, resulting in intense radar reflectivity and, thus, the retrieved values of Re , N_d , and LWC are the highest among all cloud types. Altostratus clouds are thicker and more continuous compared to altocumulus clouds, and they contain ice crystals internally, leading to higher values of Re , N_d , and LWC compared to altocumulus clouds. On clear days, cumulus and stratus clouds exhibit similar microphysical properties, but when cumulus clouds develop vigorously, the droplet radius tends to be larger than that of stratus clouds.

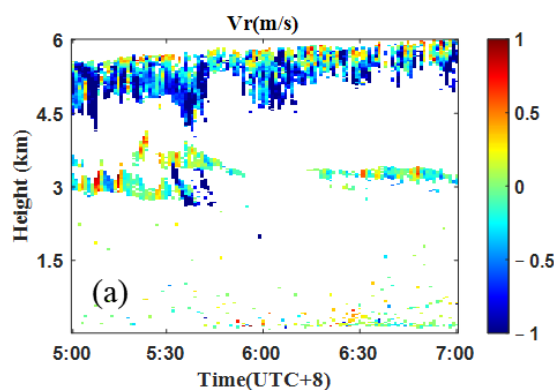


Figure 9. Cont.

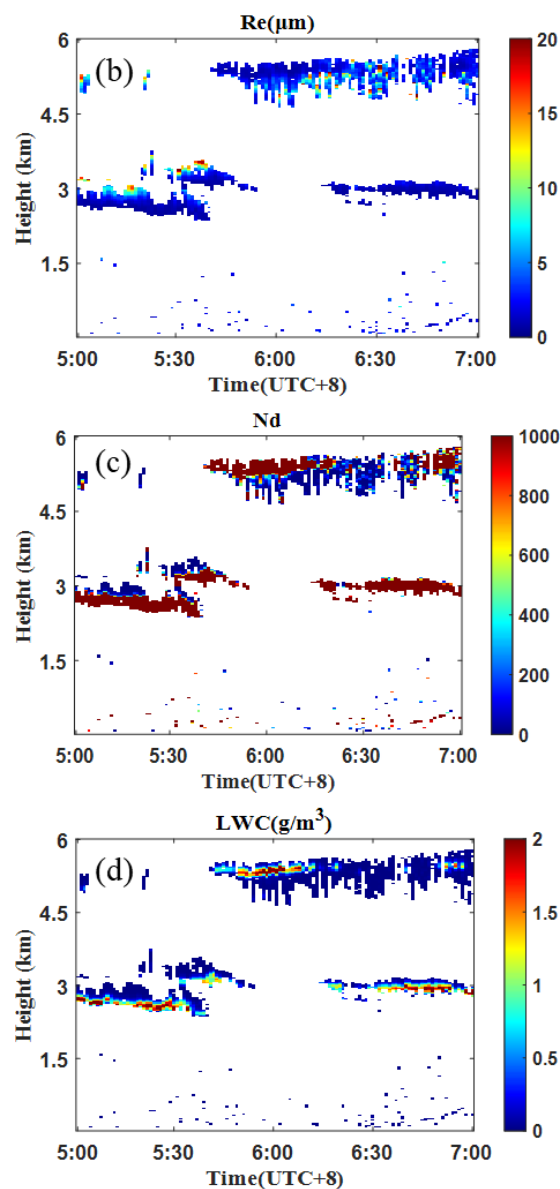


Figure 9. The MMWR observations and combined retrieval results at the Shanghai World Expo Park on 1 November 2020 for (a) radial velocity, (b) effective radius, (c) number concentration, and (d) liquid water content.

Table 2. The retrieved microphysical properties of different cloud types observed at the Shanghai World Expo Park from May to November 2021 (ice clouds with cloud base height above 6 km were excluded, and cloud droplets with retrieved Re less than $2.5 \mu\text{m}$ were considered aerosol and excluded). Ac represents altocumulus, As represents altostratus, Ns represents nimbostratus, and Cu represents cumulus.

Date	Cloud Type	$Re(\mu\text{m})$		$Nd(\text{cm}^{-3})$		$LWC(\text{g}\cdot\text{m}^{-3})$	
		Max	Mean	Max	Mean	Max	Mean
6 May 2021	Ac	36.21	7.30	9678	530	0.61	0.05
7 May 2021	Ac	7.48	3.27	23,160	4373	1.18	0.30
24 May 2021	As	62.43	6.35	125,014	4636	6.26	0.37
4 June 2021	As	55.52	8.72	14,897	745	0.90	0.08
20 June 2021	Ac	65.27	9.47	61,114	1808	4.04	0.16
31 July 2021	Ns	91.53	9.55	215,295	4321	11.85	0.34

Table 2. Cont.

Date	Cloud Type	Re(μm)		Nd (cm^{-3})		LWC ($\text{g}\cdot\text{m}^{-3}$)	
		Max	Mean	Max	Mean	Max	Mean
13 August 2021	Cu	51.72	6.98	36,999	829	2.27	0.08
8 September 2021	Cu	60.17	7.77	79,472	1646	4.03	0.17
6 October 2021	Cu→Ns	66.83	9.21	50,275	1266	3.39	0.13
18 October 2021	Ns	79.30	7.26	331,230	2545	16.62	0.28
2 November 2021	Ac	46.04	7.26	41,250	1840	2.22	0.18
13 November 2021	As	70.14	8.49	347,521	9928	17.39	0.78
16 November 2021	As→Ns	147.06	12.46	1,162,432	10,434	88.34	1.17
17 November 2021	As	69.41	7.48	122,929	3509	6.83	0.39
18 November 2021	As	27.95	8.38	2265	95	0.12	0.01
23 November 2021	As	37.61	6.56	22,057	441	1.39	0.03
total		147.06	7.91	1,162,432	3059	88.34	0.28

5. Conclusions

We presented a new method for retrieving cloud microphysical properties using both MMWR and lidar. Based on the theory of wavelength-dependent backscattering of clouds with the same particle size, we estimated the Re of cloud droplets and then combined it with the lidar-derived extinction coefficient to calculate the Nd and LWC of cloud droplets. The LWP calculated using the combined retrieval method is consistent with that obtained using microwave radiometers, indicating the reliability of the combined retrieval. Sensitivity analysis was also performed to determine the appropriate extinction backscatter ratio for the combined retrieval of cloud microphysical properties at the Shanghai World Expo Park. Finally, we studied the process of a stratus, and the results show that the cloud was a typical non-precipitating low-level water cloud.

From the results, the combined retrieval approach outperformed the retrieval results from the MMWR and reduced the reliance on assuming cloud droplet size distributions, thus minimizing their impact on the retrieval results. However, the combined retrieval method also has its limitations: (1) The geographical separation between the MMWR and lidar introduces a time delay in receiving the cloud signals, resulting in retrieval errors. (2) The lidar has limited penetration capability, especially when faced with thick cloud layers, leading to weak or even no echo signals and larger retrieval deviations. In future research, we will make efforts to address these two limitations and further investigate aerosol–cloud interactions using the retrieved cloud microphysical properties.

Author Contributions: Conceptualization, methodology, W.L., Q.H. and T.C.; data curation, Q.H., H.C. and C.L.; resources, Q.H., J.L., Z.H., Y.G. and X.H.; formal analysis, W.L.; software, W.L. and Q.H.; writing—original draft preparation, W.L.; writing—review and editing, W.L., Q.H. and T.C.; funding acquisition, T.C. and Q.H. All authors have read and agreed to the published version of the manuscript.

Funding: This research was jointly supported by the National Key Research and Development Program of China (2023YFC3708202), the National Natural Science Foundation of China (42330603, 42175179), the Natural Science Foundation of Shanghai (22ZR1404000), and the Science and Technology Planning Program of Xinjiang, China (Grant No. 2022E01047).

Data Availability Statement: Any data that support the findings of this study are included within the article. Data will be made available on request.

Acknowledgments: We sincerely appreciate the millimeter-wave radar, lidar, and microwave radiometer data provided by Shanghai World Expo Park. We acknowledge the use of MATLAB R2003a software. We would like to thank the anonymous reviewers for their helpful suggestions.

Conflicts of Interest: The authors declare no conflicts of interest.

References

1. Stocker, T.F.; Qin, D.; Plattner, G.K.; Tignor, M.; Allen, S.K.; Boschung, J.; Nauels, A.; Xia, Y.; Bex, V.; Midgley, P.M. *Climate Change 2013: The Physical Science Basis. Contribution of Working Group I to the Fifth Assessment Report of the Intergovernmental Panel on Climate Change*; Cambridge University Press: Cambridge, UK; New York, NY, USA, 2013; pp. 335–344.
2. Rosenfeld, D.; Sherwood, S.; Wood, R.; Donner, L. Climate Effects of Aerosol-Cloud Interactions. *Science* **2014**, *343*, 379–380. [[CrossRef](#)]
3. Bony, S.; Stevens, B.; Frierson, D.M.W.; Jakob, C.; Kageyama, M.; Pincus, R.; Shepherd, T.G.; Sherwood, S.C.; Siebesma, A.P.; Sobel, A.H.; et al. Clouds, Circulation and Climate Sensitivity. *Nat. Geosci.* **2015**, *8*, 261–268. [[CrossRef](#)]
4. Webb, M.J.; Andrews, T.; Bodas-Salcedo, A.; Bony, S.; Bretherton, C.S.; Chadwick, R.; Chepfer, H.; Douville, H.; Good, P.; Kay, J.E.; et al. The Cloud Feedback Model Intercomparison Project (Cfmip) Contribution to Cmpip6. *Geosci. Model Dev.* **2017**, *10*, 359–384. [[CrossRef](#)]
5. Hartmann, D.L.; Ockertbell, M.E.; Michelsen, M.L. The Effect of Cloud Type on Earths Energy-Balance—Global Analysis. *J. Clim.* **1992**, *5*, 1281–1304. [[CrossRef](#)]
6. Ockertbell, M.E.; Hartmann, D.L. The Effect of Cloud Type on Earths Energy-Balance—Results for Selected Regions. *J. Clim.* **1992**, *5*, 1157–1171. [[CrossRef](#)]
7. Carslaw, K.S.; Lee, L.A.; Reddington, C.L.; Pringle, K.J.; Rap, A.; Forster, P.M.; Mann, G.W.; Spracklen, D.V.; Woodhouse, M.T.; Regayre, L.A.; et al. Large Contribution of Natural Aerosols to Uncertainty in Indirect Forcing. *Nature* **2013**, *503*, 67–71. [[CrossRef](#)]
8. Sun, L.; Wei, J.; Wang, J.; Mi, X.; Guo, Y.; Lv, Y.; Yang, Y.; Gan, P.; Zhou, X.; Jia, C.; et al. A Universal Dynamic Threshold Cloud Detection Algorithm (Udtdca) Supported by a Prior Surface Reflectance Database. *J. Geophys. Res. Atmos.* **2016**, *121*, 7172–7196. [[CrossRef](#)]
9. Kotarba, A.Z. Impact of Moderate Resolution Imaging Spectroradiometer (Modis) Cloud Mask Interpretation on Cloud Amount Estimation. *J. Geophys. Res. Atmos.* **2015**, *120*, 8971–8986. [[CrossRef](#)]
10. Costantino, L.; Bréon, F.M. Aerosol Indirect Effect on Warm Clouds over South-East Atlantic, from Co-Located Modis and Calipso Observations. *Atmos. Chem. Phys.* **2013**, *13*, 69–88. [[CrossRef](#)]
11. Wang, Y.; Zhao, C.F. Can Modis Cloud Fraction Fully Represent the Diurnal and Seasonal Variations at Doe Arm Sgp and Manus Sites? *J. Geophys. Res. Atmos.* **2017**, *122*, 329–343. [[CrossRef](#)]
12. Gossard, E.E.; Snider, J.B.; Clothiaux, E.E.; Martner, B.; Gibson, J.S.; Kropfli, R.A.; Frisch, A.S. The Potential of 8-Mm Radars for Remotely Sensing Cloud Drop Size Distributions. *J. Atmos. Ocean. Technol.* **1997**, *14*, 76–87. [[CrossRef](#)]
13. Austin, R.T.; Heymsfield, A.J.; Stephens, G.L. Retrieval of Ice Cloud Microphysical Parameters Using the Cloudsat Millimeter-Wave Radar and Temperature. *J. Geophys. Res. Atmos.* **2009**, *114*, 19. [[CrossRef](#)]
14. Zhao, C.F.; Qiu, Y.M.; Dong, X.B.; Wang, Z.; Peng, Y.; Li, B.; Wu, Z.; Wang, Y. Negative Aerosol-Cloud re Relationship from Aircraft Observations over Hebei, China. *Earth Space Sci.* **2018**, *5*, 19–29. [[CrossRef](#)]
15. Boers, R.; Russchenberg, H.; Erkelens, J.; Venema, V.; van Lammeren, A.; Apituley, A.; Jongen, S. Ground-Based Remote Sensing of Stratocumulus Properties during Clara, 1996. *J. Appl. Meteorol.* **2000**, *39*, 169–181. [[CrossRef](#)]
16. Weitkamp, C. (Ed.) *Lidar: Range-Resolved Optical Remote Sensing of the Atmosphere*; Springer Series on Optical Science; Springer: New York, NY, USA, 2005.
17. O'Connor, E.J.; Hogan, R.J.; Illingworth, A.J. Retrieving Stratocumulus Drizzle Parameters Using Doppler Radar and Lidar. *J. Appl. Meteorol.* **2005**, *44*, 14–27. [[CrossRef](#)]
18. Intrieri, J.M.; Stephens, G.L.; Eberhard, W.L.; Uttal, T. A Method for Determining Cirrus Cloud Particle Sizes Using Lidar and Radar Backscatter Technique. *J. Appl. Meteorol.* **1993**, *32*, 1074–1082. [[CrossRef](#)]
19. Mitrescu, C.; Haynes, J.M.; Stephens, G.L.; Miller, S.D.; Heymsfield, G.M.; McGill, M.J. Cirrus Cloud Optical, Microphysical, and Radiative Properties Observed during the Crystal-Face Experiment: A Lidar-Radar Retrieval System. *J. Geophys. Res. Atmos.* **2005**, *110*, 17. [[CrossRef](#)]
20. Protat, A.; Delanoë, J.; O'Connor, E.J.; L'Ecuyer, T.S. The Evaluation of CloudSat and CAPLISO Ice Microphysical Products Using Ground-Based Cloud Radar and Lidar Observations. *J. Atmos. Ocean. Technol.* **2010**, *27*, 793–810. [[CrossRef](#)]
21. Vivekanandan, J.; Ghatge, V.P.; Jensen, J.B.; Ellis, S.M.; Schwartz, M.C. A Technique for Estimating Liquid Droplet Diameter and Liquid Water Content in Stratocumulus Clouds Using Radar and Lidar Measurements. *J. Atmos. Ocean. Technol.* **2020**, *37*, 2145–2161. [[CrossRef](#)]
22. Heymsfield, A.J.; Protat, A.; Bouniol, D.; Austin, R.T.; Hogan, R.J.; Delanoë, J.; Okamoto, H.; Sato, K.; van Zadelhoff, G.-J.; Donovan, D.P.; et al. Testing Iwc Retrieval Methods Using Radar and Ancillary Measurements with in Situ Data. *J. Appl. Meteorol. Climatol.* **2008**, *47*, 135–163. [[CrossRef](#)]
23. Delanoë, J.; Hogan, R.J. A Variational Scheme for Retrieving Ice Cloud Properties from Combined Radar, Lidar, and Infrared Radiometer. *J. Geophys. Res. Atmos.* **2008**, *113*, 21. [[CrossRef](#)]
24. Gossard, E.E. Measurement of Cloud Droplet Size Spectra by Doppler Radar. *J. Atmos. Ocean. Technol.* **1994**, *11*, 712–726. [[CrossRef](#)]
25. Tao, F. Research on Particle Spectrum Retrieval and Application Based on Millimeter Wave Cloud Radar. Ph.D. Thesis, Nanjing University of Information Science and Technology, Nanjing, China, 2021. (In Chinese).
26. He, Q.S.; Li, C.C.; Mao, J.T.; Lau, A.K.H.; Li, P.R. A Study on the Aerosol Extinction-to-Backscatter Ratio with Combination of Micro-Pulse Lidar and Modis over Hong Kong. *Atmos. Chem. Phys.* **2006**, *6*, 3243–3256. [[CrossRef](#)]

27. Huang, X.Y.; Zhang, S.; Li, Y.Y.; Huang, J.H.; Wang, P. Study on the two algorithms and result comparison of retrieving cloud microphysical parameters with ground-based radar. *J. Meteorol. Sci.* **2019**, *39*, 608–616. (In Chinese)
28. Shupe, M.D.; Kollias, P.; Poellot, M.; Eloranta, E. On Deriving Vertical Air Motions from Cloud Radar Doppler Spectra. *J. Atmos. Ocean. Technol.* **2008**, *25*, 547–557. [[CrossRef](#)]
29. Moise, T.; Flores, J.M.; Rudich, Y. Optical Properties of Secondary Organic Aerosols and Their Changes by Chemical Processes. *Chem. Rev.* **2015**, *115*, 4400–4439. [[CrossRef](#)] [[PubMed](#)]
30. Welton, E.J.; Voss, K.J.; Gordon, H.R.; Maring, H.; Smirnov, A.; Holben, B.; Schmid, B.; Livingston, J.M.; Russell, P.B.; Durkee, P.A.; et al. Ground-Based Lidar Measurements of Aerosols during Ace-2: Instrument Description, Results, and Comparisons with Other Ground-Based and Airborne Measurements. *Tellus Ser. B-Chem. Phys. Meteorol.* **2000**, *52*, 636–651. [[CrossRef](#)]
31. He, Q.S. Remote Sensing of Tropospheric Aerosol Optical Properties and Distribution Characteristics by Micro Pulse Lidar. Ph.D. Thesis, Peking University, Beijing, China, 2006. (In Chinese).
32. Schmidt, J.; Wandinger, U.; Malinka, A. Dual-Field-of-View Raman Lidar Measurements for the Retrieval of Cloud Microphysical Properties. *Appl. Opt.* **2013**, *52*, 2235–2247. [[CrossRef](#)]
33. Schmidt, J.; Ansmann, A.; Bühl, J.; Baars, H.; Wandinger, U.; Mueller, D.; Malinka, A.V. Dual-Fov Raman and Doppler Lidar Studies of Aerosol-Cloud Interactions: Simultaneous Profiling of Aerosols, Warm-Cloud Properties, and Vertical Wind. *J. Geophys. Res. Atmos.* **2014**, *119*, 5512–5527. [[CrossRef](#)]
34. Lu, M.L.; Seinfeld, J.H. Effect of Aerosol Number Concentration on Cloud Droplet Dispersion: A Large-Eddy Simulation Study and Implications for Aerosol Indirect Forcing. *J. Geophys. Res. Atmos.* **2006**, *111*, 16. [[CrossRef](#)]
35. Crewell, S.; Löhnert, U. Accuracy of Cloud Liquid Water Path from Ground-Based Microwave Radiometry: 2: Sensor Accuracy and Synergy: Art. No. 8042. *Radio Sci.* **2003**, *3*, 11.
36. Westwater, E.R. The Accuracy of Water-Vapor and Cloud Liquid Determination by Dual-Frequency Ground-Based Microwave Radiometry. *Radio Sci.* **1978**, *13*, 677–685. [[CrossRef](#)]
37. Wang, N.C.; Zhang, K.; Shen, X.; Wang, Y.; Li, J.; Li, C.; Mao, J.; Malinka, A.; Zhao, C.; Russell, L.M.; et al. Dual-Field-of-View High-Spectral-Resolution Lidar: Simultaneous Profiling of Aerosol and Water Cloud to Study Aerosol-Cloud Interaction. *Proc. Natl. Acad. Sci. USA* **2022**, *119*, 9. [[CrossRef](#)] [[PubMed](#)]
38. Jimenez, C.; Ansmann, A.; Engelmann, R.; Donovan, D.; Malinka, A.; Schmidt, J.; Seifert, P.; Wandinger, U. The Dual-Field-of-View Polarization Lidar Technique: A New Concept in Monitoring Aerosol Effects in Liquid-Water Clouds—Theoretical Framework. *Atmos. Chem. Phys.* **2020**, *20*, 15247–15263. [[CrossRef](#)]
39. Greenwald, T.J.; Stephens, G.L.; Christopher, S.A.; Haar, T.H.V. Observations of the Global Characteristics and Regional Radiative Effects of Marine Cloud Liquid Water. *J. Clim.* **1995**, *8*, 2928–2946. [[CrossRef](#)]
40. Zheng, X.J.; Xi, B.K.; Dong, X.Q.; Logan, T.; Wang, Y.; Wu, P. Investigation of Aerosol-Cloud Interactions under Different Absorptive Aerosol Regimes Using Atmospheric Radiation Measurement (Arm) Southern Great Plains (Sgp) Ground-Based Measurements. *Atmos. Chem. Phys.* **2020**, *20*, 3483–3501. [[CrossRef](#)]

Disclaimer/Publisher’s Note: The statements, opinions and data contained in all publications are solely those of the individual author(s) and contributor(s) and not of MDPI and/or the editor(s). MDPI and/or the editor(s) disclaim responsibility for any injury to people or property resulting from any ideas, methods, instructions or products referred to in the content.